

1 Single-blind test of airplane-based hyperspectral methane detection via 2 controlled releases

3 Evan D. Sherwin^{1,†,*}, Yuanlei Chen^{1,†}, Arvind P. Ravikumar², Adam R. Brandt¹

4 ¹Department of Energy Resources Engineering, Stanford University, Stanford, California, USA

5 ²Department of Systems Engineering, Harrisburg University of Science and Technology, Harrisburg, Pennsylvania, USA

6 ³† Denotes equal contribution

7 *evands@stanford.edu

8 **Abstract**

9 Methane leakage from point sources in the oil and gas industry is a major contributor to global greenhouse
10 gas emissions. The majority of such emissions come from a small fraction of “super-emitting” sources.
11 We evaluate the emission detection and quantification capabilities of Kairos Aerospace’s airplane-based
12 hyperspectral imaging methane emission detection system. In blinded controlled releases of methane con-
13 ducted over four days in San Joaquin County, California, USA, Kairos detected 182 of 200 valid nonzero
14 releases, including all 173 over 15 kilograms per hour of methane ($\text{kg}(\text{CH}_4)$) per meter per second
15 (mps) of wind and none of the 12 nonzero releases below $8.3 \text{ kg}(\text{CH}_4)/\text{mps}$. 9 of the 26 releases in the
16 partial detection range of 5 to $15 \text{ kg}(\text{CH}_4)/\text{mps}$ were detected. There were no false positives: Kairos
17 did not detect methane during any of the 21 negative controls. Plume quantification accuracy depends on
18 the wind measurement technique, with a parity slope of 1.15 ($\sigma=0.037$, $R^2=0.84$, $N=185$) using a cup-
19 based wind meter and 1.45 ($\sigma=0.059$, $R^2=0.80$, $N=157$) using an ultrasonic anemometer. Performance is
20 comparable even with only modeled wind data. Quantification error scales roughly as a fixed percentage
21 of emission size. These findings suggest that at 2 mps winds under favorable environmental conditions
22 in the US, Kairos could detect and quantify over 50% of total emissions by identifying super-emitting
23 sources.

24 **Introduction**

25 US natural gas (NG) production reached 110 billion cubic feet per day (bcfd) in August 2019, a 56%
26 increase over the past decade EIA (2019). The shift from coal toward less carbon-intensive NG and
27 renewables has reduced the carbon intensity of the US power sector Schivley et al. (2018). However, the
28 climate benefits of NG cannot be fully realized if methane leaks into the atmosphere at significant rates,
29 as methane has a global warming potential that is 28-36 times that of carbon dioxide over a 100-year
30 period EPA (2017).

31 The US Environmental Protection Agency (EPA) greenhouse gas inventory states that NG and
32 petroleum systems accounted for 32% of total US methane emissions and about 4% of total US green-
33 house gas emissions in 2017 EPA (2019). Field surveys in gas-producing regions suggest that the EPA
34 inventory underestimates NG methane emissions, likely because EPA’s process-based approach does not
35 sufficiently account for emissions from extremely large sources Brandt et al. (2014); Lyon et al. (2016);
36 Zavala-Araiza et al. (2015). Emission sizes in the North American NG supply chain are found to fol-
37 low a heavy-tailed distribution, where the top 5% of point sources, so-called “super-emitters”, contribute
38 over 50% of total emissions Brandt et al. (2014). A recent study indicates that 10% of the methane point

39 sources in California, including oil and gas facilities, landfills, wastewater treatment plants, and dairy
40 manure management sites, are responsible for 60% of the detected point-source emissions Duren et al.
41 (2019). Therefore, leak detection and repair (LDAR) programs could reduce the cost of detection and
42 mitigation by allowing mitigation efforts to focus on the largest sources. Given the limited resources and
43 manpower available for detection and repair, technologies for rapidly and accurately identifying super-
44 emitters are essential for guiding mitigation efforts.

45 Close-range approaches, such as optical gas imaging, are widely employed in ground-based LDAR
46 programs in the oil and gas industry. These methods are effective for source identification Ravikumar
47 et al. (2018), but can be slow and labor-intensive. Mobile systems with sensors placed on trucks, drones,
48 or aircraft have the potential advantage of speeding up detection by avoiding the need for manual detec-
49 tion via in-person site visits Ravikumar et al. (2019). In particular, mobile remote sensing via airplanes
50 or satellites can be used to target super-emitters, providing benefits of “low per-site cost, high spatial
51 coverage, and frequent sampling” Fox et al. (2019).

52 We examine a system developed by Kairos Aerospace (henceforth “Kairos”). Kairos’ LeakSurveyor
53 is a hyperspectral methane imaging system that is mounted on a light aircraft flown at general aviation
54 altitudes of approximately 900 m (3,000 feet) above ground level. The system uses an infrared imaging
55 spectrometer to detect methane, an optical camera to create an optical surface map of the surveyed region,
56 and GPS and inertial measurement units to record the position and orientation of the sensor Kairos (2019).
57 This system is capable of surveying roughly 400 square kilometers (150 square miles) of oil and gas
58 infrastructure in a single day Kairos (2019). See Supplementary Information (SI) section S1 for further
59 detail.

60 This study performs large-volume single-blind controlled releases, motivated in part by the Mobile
61 Monitoring Challenge (MMC), organized by the Stanford Natural Gas Initiative and the Environmental
62 Defense Fund (EDF). The 2018 MMC tested ten methane detection technologies through single-blind
63 controlled releases, with 6 out of the 10 participating technologies “correctly detecting over 90% of test
64 scenarios (true positive plus true negative rates)” Ravikumar et al. (2019).

65 In contrast, we focus on characterizing quantification accuracy of the super-emitting methane point
66 sources that Kairos’ technology was designed to quickly identify through aerial surveys. As a result,
67 our emission rates are two to three orders of magnitude larger than those in the MMC, reaching over
68 1,000 kilograms of methane per hour ($\text{kg}(\text{CH}_4)$), as opposed to 0.29 $\text{kg}(\text{CH}_4)$ for most near-ground
69 technologies in the MMC and 29 $\text{kg}(\text{CH}_4)$ for two airplane and truck-based technologies Ravikumar
70 et al. (2019).

71 **Materials and Methods**

72 *Airplane-based methane sensing technology*

73 Kairos’ methane detection technology uses hyperspectral imaging from the wing of a small aircraft to
74 construct a two-dimensional image of methane concentrations integrated along the path between the
75 airplane and the ground. Each image is generated through a single pass over an area. Kairos’ automated
76 processing identifies methane plumes and calculates a wind-adjusted methane emission rate in kilograms
77 of methane per hour per meter per second of wind ($\text{kg}(\text{CH}_4)/\text{mps}$, henceforth denoted $\text{kg}(\text{CH}_4)/\text{mps}$). Note
78 that the spectrometer detects only methane and not other constituent components of natural gas, such as
79 ethane. See the SI, section S1 for further technical detail.

80 *Test location and set-up*

81 The Stanford team performed four days of single-blind controlled releases in San Joaquin County, Cal-
82 ifornia, on October 8th, 10th, 11th, and 15th, 2019. Kairos personnel were in the aircraft but were not

83 present at the ground release site. Stanford personnel designed the methane release schedule and controlled the release rates with assistance from a natural gas release operator, Rawhide Leasing.

85 We measured methane flow rates through Sierra Instruments QuadraTherm 740i thermal mass flow meters Sierra (2019). We measured wind speed and direction using both a Vantage Vue Sensor Suite with a cup-based wind meter and a Gill Instruments WindSonic 60 two-dimensional ultrasonic anemometer (not present on the first day of data collection) Davis (2018); Gill (2019). See the SI, Section S2 for further detail.

90 *Single-blind experimental design*

91 The aerial test used a two-person airplane occupied by one pilot and one Kairos engineer, with Kairos' LeakSurveyor instrument fastened to one wing strut. The Kairos engineer oversaw operations and radio communication with ground crews from Stanford and Rawhide. As the aircraft passed over the test site, the Kairos instrument attempted to detect any methane below. The aircraft flew repeated North-South round-trip passes on a fixed route, passing overhead roughly every four minutes, varying from three to five minutes depending on wind and other environmental conditions.

97 Kairos did not have access to data collected on the ground until they reported final results to Stanford on October 24th. Kairos then received actual release rates and ground-based wind measurements on October 29th. See the SI, Section S3 for further detail.

100 *Performance metrics*

101 We test Kairos' technology for detection accuracy, minimum detection threshold, and quantification accuracy. Here, detection accuracy is defined as the sum of true positive and true negative rates. The minimum detection threshold analysis characterizes both the minimum release rate that the technology can detect with some nonzero probability and the rate above which all releases are detected. Quantification accuracy compares the estimated methane release rates to the true release rate. We compute quantification accuracy using a linear fit of released v. detected methane to assess the accuracy of the detection method. For simplicity and intercomparability with other controlled release tests of methane detection technologies, we use an ordinary least squares linear regression in the main analysis, although we discuss the potential implications of weighted least squares approaches that account for variation in uncertainty across points in the SI, Section S9.

111 **Results**

112 *Data summary*

113 A total of 230 data points were collected during the four-day single-blind tests, among which 21 (~9%) were negative controls during which no methane was released. 40 releases (~17%) were dedicated to characterizing the detection threshold by releasing at a rate between 0-50 kgh. The remaining large releases (~74% of releases) were focused on testing the ability of the system to quantify high release volumes. Among these, 110 releases were within the range of 50 and 500 kgh; and 59 were over 500 kgh. Note that reported methane flow rates are 93.5% of metered natural gas flow rates PG&E (2019). The volume rates are converted to mass rates based on the molar mass of methane and the molar volume at the standard condition of 1 atm and 15 °C GPSA (2011).

121 Of the 230 data points collected, we exclude 9 from the baseline analysis due to technical issues such as an incomplete plume image or controlled release practices that deviated from protocol. 4 additional overflights did not result in valid data collection due to an incorrect flight altitude (see the SI, section S2 for details). When using wind speed from the cup meter, we exclude an additional 8 data points from

125 the 230 data points with measured 1-minute gust wind speed lower than 0.9 mps (2 miles per hour), the
126 rated uncertainty. We also exclude data points from the quantification analysis if there is not sufficient
127 time after a change in release level for full plume development. See the SI, Section S5 for further detail.

128 Figure 1 shows false color images of methane plumes detected by the Kairos instrument during the
129 trial, with blue and white representing low and high concentrations, respectively. All connected pixels
130 are considered to be within a single plume. If there are multiple disconnected plumes, we consider the
131 closest plume to the release point, consistent with Kairos' internal practices. Figure 1a shows a Kairos
132 image while no methane is being released. Figure 1b shows a small plume at a release rate of 36 kgh,
133 approaching the minimum detection threshold of the instrument. The plume in Figure 1c is clearly visible,
134 with a wind-adjusted release rate of 87 kgh. Figures 1d-f show larger plumes with a wider field of view.

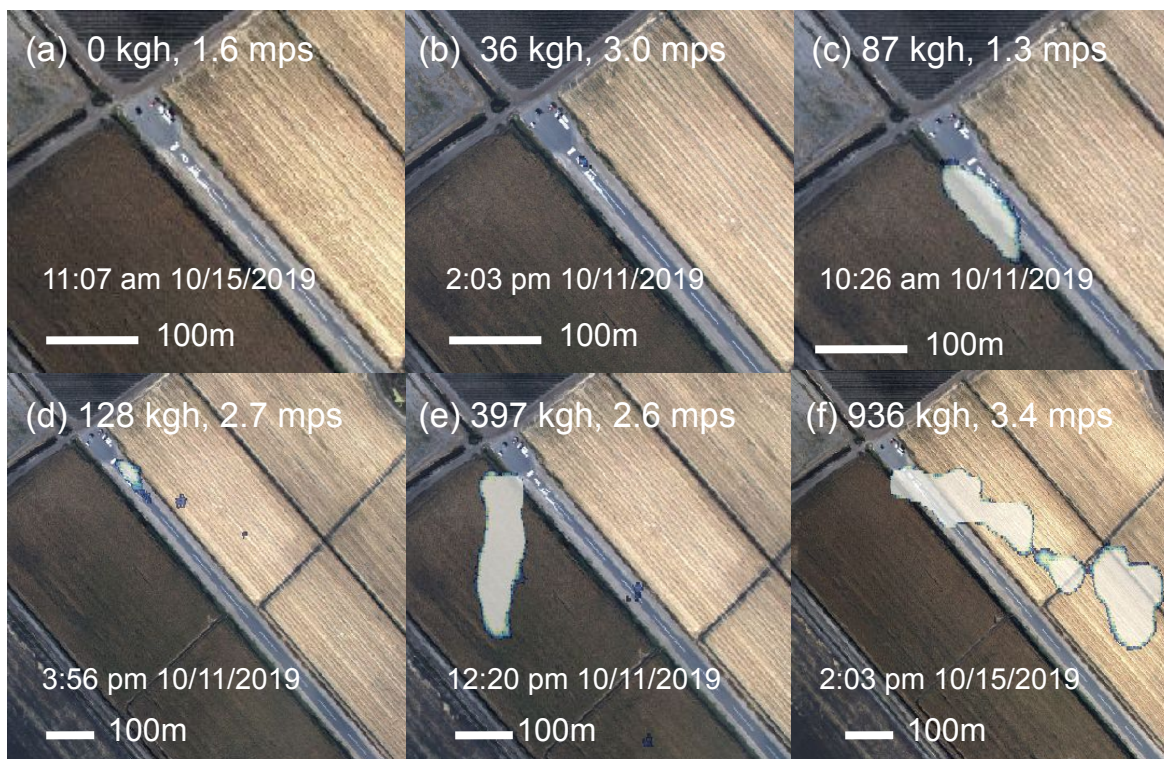


Figure 1. Examples of detected plumes associated with different methane release rates. Plumes are shown in colorized spectrometer images, with blue and white representing low and high concentrations of methane, respectively. Optical images were taken from the airplane as it passed overhead. Each image includes the measured methane release rate, in kgh, and wind speed from the ultrasonic anemometer. Note that the scale changes in the bottom row, d-f. (a) No release. (b) Small release, close to detection threshold. (c) Medium-sized release, low wind. (d) Medium-sized release, moderate wind. (e) Large emission, moderate wind. (f) Approaching maximum release rate, moderate wind.

135 *Detection probability and false positive rate*

136 Kairos previously published work reporting a 50% probability of detection at 9.2 kgh/mps Kairos (2019).
137 Considering the limited resources available for this study and the interest in testing quantification accu-
138 racy at large emission rates, only 17% of data points have nonzero release rates below 50 kgh. Due to
139 exclusion criteria and the wind speed conditions at the time of the release, 36 valid data points fall in the
140 range of 0-25 kgh/mps and are presented in Figure 2.

141 Note that we present results in these wind-normalized units for two reasons. First, Kairos' instrument
142 outputs readings in wind-normalized terms, so this presentation of results disentangles instrument capa-
143 bilities from the wind profile of the region in question. Second, these releases were on the low end of what
144 our release apparatus could accurately meter. As a result, for many of these smaller releases we left the
145 release level constant and allowed the wind to provide the variability. Thus, converting wind-normalized
146 releases to absolute methane fluxes would remove this variability.

147 Figure 2 shows the fraction of emissions detected by Kairos as a function of the wind-speed-
148 normalized methane release rate for the 35 points below 25 kgh/mps, using 1-minute gust measurements
149 from the cup wind meter. Small circles on the top and bottom of the histogram represent each emission
150 and whether it was detected. Only 1 of the 14 data points in the 5-10 kgh/mps range was detected, with
151 a true emission rate of 8.3 kgh/mps. The detection rate rises to 67% for release rates of 10-15 kgh/mps.
152 Above 15 kgh/mps, 100% of emissions were detected, both in this subsample and in the data set as a
153 whole. Thus, the 50% probability of detection threshold likely occurs between 8.3 and 15 mcfd/mph,
154 consistent with Kairos' internal trials. Error bars represent twice the standard error assuming a binomial
155 distribution, with no error bars shown for cases with 100% or 0% detection rates. This suggests that the
156 instrument can detect all emissions above about 15 kgh/mps with high probability.

157 Note that due to sensitive manual flow controls and high relative meter error and flow variability at
158 these low flow rates, for this section of the analysis we opted to hold the overall methane release rate
159 relatively constant for extended periods of time, allowing changes in wind speed to provide variability
160 in the wind-normalized release rates that Kairos' method produces. As a result, we characterize the min-
161 imum detection threshold in terms of wind-normalized methane release rates but do not have sufficient
162 variability in the overall flow rate to quantify the minimum detection threshold in terms of methane flow
163 rate.

164 To test for false positives, we devote ~9% of releases (21 releases) to negative controls with release
165 rates of 0 kgh. Kairos reported no detections during these periods, leading to a false positive rate of
166 0%. This is in part because such remote sensing techniques are less sensitive than many other methane
167 detectors, missing small emissions but rarely triggering false positives. Thus, Kairos detected all 173
168 releases over 15 kgh/mps and none of the 12 nonzero releases below 8.3 kgh/mps.

169 In all, Kairos detected 182 of 200 valid nonzero releases and had no false positives in the 21 negative
170 controls, resulting in an overall accuracy of 91.9%, with 100% accuracy for releases above 15 kgh/mps.

171 *Quantification accuracy*

172 Figure 3(a) shows 185 valid data points associated with nonzero release rates, comparing the metered
173 release rates (x-axis) to the estimated rates generated by Kairos. For consistency with Kairos' internal
174 testing procedures, we use 1-minute gust wind speed from the cup wind meter to convert the Kairos-
175 reported emission estimate in kgh/mps to kgh, using wind speed measured at the time of each pass.
176 Kairos reports point estimates with no uncertainty in kgh/mps. Uncertainties in wind measurements are
177 $\pm \sim 0.9$ mps (± 2 mile per hour) for the cup wind meter. This introduces errors in Kairos' estimates of
178 release rates due to uncertainty in wind speed, shown in the Y error bars in Figure 3(a). The length of
179 the error bars is thus dependent on the magnitude of the Kairos-reported number in kgh/mps. The y-axis
180 of Figure 3(b) shows the Kairos-reported number multiplied by 1-min gust wind speed measured with
181 the ultrasonic anemometer, which has a rated accuracy of roughly $\pm 2\%$, with some variation depending
182 on wind speed Gill (2019). In this case, the length of the error bars depends both on the magnitude of
183 the measured wind speed and the Kairos-reported quantification in kgh/mps. Although the ultrasonic
184 anemometer has a much smaller measurement uncertainty, it was not present for the first day of data
185 collection. Therefore, we use results from the cup wind meter, shown in Figure 3(a) as a baseline. See the

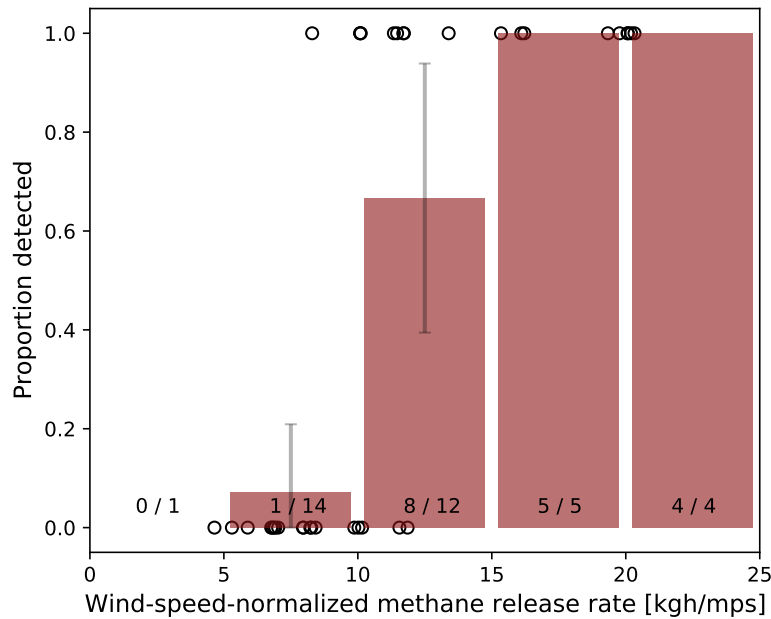


Figure 2. Binary detection results and the proportion of releases detected when the true release rates fall in the range of 0-25 kgh/mps. Each bin has a width of 5 kgh/mps. Kairos detected 100% of emissions above 15 kgh/mps. The smallest release detected was 8.3 kgh/mps. Error bars show twice the standard error assuming a binomial distribution. The fraction at the bottom of each bin denotes the number of true positives divided by the total number of releases in this range. Small circles on the top and bottom of the histogram represent each emission and whether it was detected.

186 SI, Section S6 for further detail. See the SI, Section S7 for further detail on uncertainty and variability in
187 the measured natural gas flow rate.

188 Using winds from the cup wind meter, the linear fit is relatively close to parity, with an R^2 of 0.84 and
189 a slope of 1.15 ($\sigma = 0.037$), shown in in Figure 3(a). The slope is statistically distinguishable from zero
190 at the $p=0.05$ level. This finding is robust to several techniques that correct for heteroskedasticity in the
191 data, shown in the SI, Section S9. Note that the confidence intervals in Figure 3 assume homoskedasticity,
192 which residual plots in Figure S17 suggest does not hold. Heteroskedastic confidence intervals would
193 widen further at higher release rates. Using ultrasonic anemometer wind data, R^2 drops to 0.80 and the
194 best fit line exhibits a larger slope of 1.45 ($\sigma = 0.059$), indicating somewhat more bias.

195 In the field, Kairos may not have access to on-the-ground wind measurements. In these circumstances,
196 one would likely use third-party data products to approximate local wind speed and direction. Figure
197 3(c) uses 1-minute gust wind reanalysis data from Dark Sky, a private company that estimates minute-
198 resolution wind speed at high spatial resolution across the United States based largely on publicly avail-
199 able data sources and atmospheric modeling Apple (2016). Dark Sky reports wind speed values at 10 m,
200 which we convert to 2.5 m values using a factor of $(2.5/10)^{0.15}$ for grassland terrain, based on Banuelos-
201 Ruedas et al. (2011). See the SI, Section S5.3.2 for further detail.

202 Figure 3(d) shows results using hourly surface gust data from the High-Resolution Rapid Refresh
203 (HRRR) wind reanalysis database, produced by the United States National Oceanic and Atmospheric
204 Administration NOAA (2020) averaging wind speed estimates over the nearest 9 km x 9 km area for the
205 three hours before, during, and after the Kairos measurement, based on Duren et al. (2019). For further

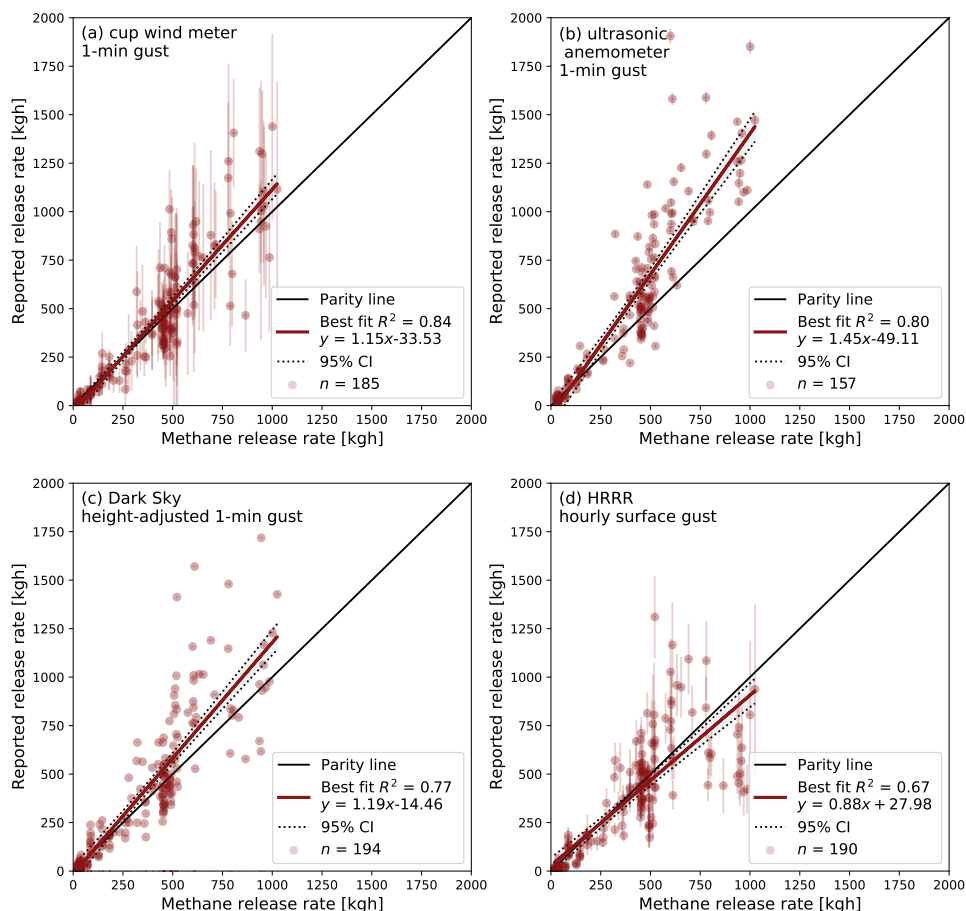


Figure 3. Parity chart of known nonzero methane release rates and the corresponding Kairos-reported estimate in kgh/mps multiplied by 1-min gust wind speed measured by (a) the cup wind meter, (b) the ultrasonic anemometer or reported by (c) height-adjusted values from the Dark Sky commercial wind reanalysis database, and (d) surface gusts from the High-Resolution Rapid Refresh (HRRR) database. The type of wind used in (a-c) is 1-minute gust wind speed. The X=Y parity line indicates perfect quantification. All four cases show a relatively close linear fit. (a-c) show mild to moderate bias toward overestimation based on minutely gust and (d) shows a mild underestimation based on hourly gust. The Dark Sky wind used in (c) is converted to 2.5-meter wind from 10-meter wind by applying a height adjustment factor. The HRRR wind used in (d) uses the method from Duren et al. (2019), averaging hourly surface gusts over three hours in the nearest 3x3 measurement locations (a box of 9 km by 9 km). See the SI, Section S5.3.2 for further detail on HRRR winds. 95% confidence intervals of the regression fits are shown. n = number of data points shown in each graph, which depends on data exclusion criteria described in the SI, Section S5.1. Y error bars are based on wind uncertainties, described in the SI, Section S6. X error bars, not visible, are based on observed flow variability and flow meter error, described in the SI, Section S7.

206 discussion of HRRR data, see the SI, Section S5.3.2. Note that (c) and (d) only exclude 6 and 10 data
207 points, respectively due to insufficient time for plume formation, while (a) excludes 15 of 200 nonzero
208 valid data points with either incomplete time for plume formation or wind speed measurements whose
209 uncertainty range contains zero. See the SI, Section S5.1 for further detail.

210 For both forms of wind reanalysis data, overall quantification performance is similar to the results
211 with ground-based wind data, with a slightly less precise linear fit. With Dark Sky in Figure 3(c), the R^2
212 falls slightly to 0.77 with a parity slope of 1.19, between the cup wind meter and ultrasonic anemometer
213 slopes. The R^2 for HRRR falls to 0.67 with a slope of 0.88, indicating average underestimates rather than
214 overestimates of total methane emissions.

215 Thus, Dark Sky data appears to provide a more precise estimate of overall emissions when ground-
216 based wind data are not available. However, because this is a proprietary product, the underlying algo-
217 rithms may change without notice. In addition, the data will likely not be publicly available after the
218 end of 2021 Grossman (2020). Although HRRR data have a lower spatial and temporal resolution, the
219 underlying process behind their production is more transparent. In addition, 15-minute HRRR data are
220 available for download within 48 hours of a given date, so future Kairos flights could likely acquire
221 publicly available HRRR data with a higher temporal resolution, potentially improving performance.

222 Although absolute residual plots in Figure S17(a-b) exhibit heteroskedasticity, percent residuals in
223 Figure S17(c-d) appear relatively stationary in release size. Analysis of the smallest and largest 50% of the
224 data (above the 100% detection threshold) demonstrates that the mean and variance are not statistically
225 distinguishable, indicating that it is reasonable to assume that percent measurement error is roughly
226 stationary as methane emission size increases. See the SI, Section S7 for further detail.

227 These results demonstrate a high level of detector performance, even without on-the-ground wind
228 measurements, in terms of high R^2 and low bias compared to past controlled releases for mobile methane
229 detectors in Ravikumar et al. (2019); Duren et al. (2019); Schwietzke et al. (2019); Conley et al. (2017)
230 and Foster-Wittig et al. (2015). That said, most controlled release studies operate at one to two orders of
231 magnitude lower release volumes with smaller sample sizes predominantly clustered near the minimum
232 detection threshold and most do not appear to employ a blinded experimental design. See the SI, Section
233 S8 for further detail.

234 *Estimate of field efficacy*

235 Using a bottom-up inventory of 1,009 methane emission sites from the US oil and gas system from
236 Omara et al. (2018), a compilation of data from nine separate studies and eight oil and gas-producing
237 basins, we estimate that given 2 mps winds and emission detection fractions based on the probabilities
238 from Figure 2, adoption of this technology would detect 53% of total emissions, with 49% coming from
239 24 sites above the 100% detection threshold of 15 kg/h/mps. At 1 mps winds, this rises to 63% of total
240 emissions. At 4 mps winds, this falls to 41% of total emissions. At 7 mps, the maximum wind speed at
241 which it is safe for these airplane-based surveys, Kairos would still detect 32% of total emissions. Note
242 that this inventory combines emissions from multiple basins. In practice, detector efficacy would likely
243 vary across basins due to different emission profiles. In addition, we do not perform a full stochastic
244 techno-economic analysis, such as that in the Fugitive Emissions Abatement Simulation Toolkit, which
245 would be necessary to determine the cost-effective mitigation potential of airplane-based methane sensing
246 technology Kemp et al. (2016).

247 **Discussion**

248 These results suggest that in suitable contexts, aerial surveys at modest wind speeds could detect 50%
249 or more of total methane emissions even without ground-based wind measurements. This process can

250 screen assets much more rapidly than traditional leak detection and repair methods, with few if any
251 resource-diverting false positives. Thus, this technology could provide rapid detection of super-emitting
252 methane leaks in upstream and midstream oil and gas, likely as a supplement to more precise but more
253 labor-intensive leak detection and repair programs. More sensitive instruments would likely be required
254 for most distribution system applications.

255 The overall cost of this field trial was roughly \$50,000 including materials, natural gas release equip-
256 ment rental, gas, and personnel, flight time, space rental, and miscellaneous expenses (not including
257 Stanford researchers' time). Given that basin-wide or state-wide aerial methane emissions survey cam-
258 paigns can cost \$1 million or more, we feel that testing the new instruments with blinded controlled
259 releases at a range of methane emission levels approaching those expected in the field, with a sample
260 size of at least a few dozen, would increase confidence in the capabilities of these methods, thus adding
261 substantial value to the data from such field campaigns.

262 **Contributions**

263 Substantial contributions to conception and design: EDS, YC, APR, ARB

264 Acquisition of data: EDS, YC

265 Analysis and interpretation of data: EDS, YC, ARB

266 Drafting the article or revising it critically for important intellectual content: EDS, YC, APR, ARB

267 Final approval of the version to be published: EDS, YC, APR, ARB

268 **Acknowledgement**

269 The authors would like to thank Jingfan Wang, Jeffrey Rutherford, and Alison L. Marsden at Stanford,
270 and Jeff Gamble and Walter Godsil from Rawhide Leasing for help with the controlled release, as well
271 as Chris Field, Jennifer Johnson, Eric Kort, Keith Andre, and Jon Carlson for their support with wind
272 measurements. We gratefully acknowledge the assistance of Tony Ramirez and the staff of Zuckerman
273 Family Farms.

274 **Funding information**

275 This study was funded by the Stanford Natural Gas Initiative, an industry consortium that supports inde-
276 pendent research at Stanford University. No funding was provided by participating or tested companies.

277 **Competing interests**

278 The authors have no competing interests to declare

279 **Supplemental material**

280 The supplemental materials for this article can be found as follows:

- 281 • **Text S1.** Supplementary Information for Single-blind test of airplane-based hyperspectral methane
282 detection via controlled releases. <https://osf.io/vqnpb/>
 - 283 – **S1.** Kairos Aerospace technology
 - 284 – **S2.** Controlled release set-up
 - 285 – **S3.** Single-blind experimental design
 - 286 – **S4.** Methane content and density
 - 287 – **S5.** Data exclusion, sensitivity analysis
 - 288 – **S6.** Wind variability and uncertainty

- 289 – **S7.** Flow variability and uncertainty
290 – **S8.** Addressing heteroskedasticity

291 **Data accessibility statement**

292 All data and code required to reproduce the results of this article are available on GitHub at:
293 [https://github.com/yuliachen/Single-blind-test-of-airplane-based-hyperspectral-methane-detection-via-](https://github.com/yuliachen/Single-blind-test-of-airplane-based-hyperspectral-methane-detection-via-controlled-releases)
294 [controlled-releases](https://github.com/yuliachen/Single-blind-test-of-airplane-based-hyperspectral-methane-detection-via-controlled-releases)

295 **References**

- 296 Apple. 2016. Dark Sky Data Sources. *Apple Inc* <https://darksky.net/dev/docs/sources>.
- 297 Banuelos-Ruedas F, Angeles-Camacho C, Rios-Marcuello S. 2011. Methodologies Used in the Extrapolation of
298 Wind Speed Data at Different Heights and Its Impact in the Wind Energy Resource Assessment in a Region.
299 *Wind Farm - Technical Regulations, Potential Estimation and Siting Assessment* doi:10.5772/20669.
- 300 Brandt AR, Heath GA, Kort EA, O’Sullivan F, Petron G, et al. 2014. Methane Leaks from North American Nat-
301 ural Gas Systems. *Science* **343**(6172): 733–735. ISSN 0036-8075, 1095-9203. doi:10.1126/science.1247045.
302 <http://www.sciencemag.org/cgi/doi/10.1126/science.1247045>.
- 303 Conley S, Faloona I, Mehrotra S, Suard M, Lenschow DH, et al. 2017. Application of Gauss’s theorem to quantify
304 localized surface emissions from airborne measurements of wind and trace gases. *Atmospheric Measurement*
305 *Techniques* **10**(9): 3345–3358. ISSN 1867-8548. doi:10.5194/amt-10-3345-2017. [https://www.atmos-](https://www.atmos-meas-tech.net/10/3345/2017/)
306 [meas-tech.net/10/3345/2017/](https://www.atmos-meas-tech.net/10/3345/2017/).
- 307 Davis. 2018. Vantage Vue Weather Station. *Davis Instruments* [https://www.davisinstruments.com/](https://www.davisinstruments.com/product_documents/weather/spec_sheets/6250_6351_57_SS.pdf)
308 [product_documents/weather/spec_sheets/6250_6351_57_SS.pdf](https://www.davisinstruments.com/product_documents/weather/spec_sheets/6250_6351_57_SS.pdf).
- 309 Duren RM, Thorpe AK, Foster KT, Rafiq T, Hopkins FM, et al. 2019. California’s methane super-emitters. *Na-*
310 *ture* **575**(7781): 180–184. ISSN 0028-0836, 1476-4687. doi:10.1038/s41586-019-1720-3. [http://www.](http://www.nature.com/articles/s41586-019-1720-3)
311 [nature.com/articles/s41586-019-1720-3](http://www.nature.com/articles/s41586-019-1720-3).
- 312 EIA. 2019. Monthly Crude Oil and Natural Gas Production. *US Energy Information Administration* (EIA-914).
313 <https://www.eia.gov/petroleum/production/#ng-tab>.
- 314 EPA. 2017. Greenhouse Gas Emissions: Understanding Global Warming Potentials. *US Environmental Pro-*
315 *tection Agency* [https://www.epa.gov/ghgemissions/understanding-global-warming-](https://www.epa.gov/ghgemissions/understanding-global-warming-potentials)
316 [potentials](https://www.epa.gov/ghgemissions/understanding-global-warming-potentials).
- 317 EPA. 2019. Inventory of U.S. Greenhouse Gas Emissions and Sinks: 1990-2017. *United States Environmental Pro-*
318 *tection Agency* (EPA430-R-19-001). [https://www.epa.gov/sites/production/files/2019-](https://www.epa.gov/sites/production/files/2019-04/documents/us-ghg-inventory-2019-main-text.pdf)
319 [04/documents/us-ghg-inventory-2019-main-text.pdf](https://www.epa.gov/sites/production/files/2019-04/documents/us-ghg-inventory-2019-main-text.pdf).
- 320 Foster-Wittig TA, Thoma ED, Albertson JD. 2015. Estimation of point source fugitive emission rates from a single
321 sensor time series: A conditionally-sampled Gaussian plume reconstruction. *Atmospheric Environment* **115**:
322 101–109. ISSN 13522310. doi:10.1016/j.atmosenv.2015.05.042. [https://linkinghub.elsevier.](https://linkinghub.elsevier.com/retrieve/pii/S135223101530114X)
323 [com/retrieve/pii/S135223101530114X](https://linkinghub.elsevier.com/retrieve/pii/S135223101530114X).
- 324 Fox TA, Barchyn TE, Risk D, Ravikumar AP, Hugenholtz CH. 2019. A review of close-range and screening
325 technologies for mitigating fugitive methane emissions in upstream oil and gas. *Environmental Research*
326 *Letters* **14**(5): 053002. ISSN 1748-9326. doi:10.1088/1748-9326/ab0cc3. [https://iopscience.iop.](https://iopscience.iop.org/article/10.1088/1748-9326/ab0cc3)
327 [org/article/10.1088/1748-9326/ab0cc3](https://iopscience.iop.org/article/10.1088/1748-9326/ab0cc3).
- 328 Gill. 2019. Wind Speed & Direction Sensor. *Gill Instruments* [http://gillinstruments.com/data/](http://gillinstruments.com/data/datasheets/windsonic-1405-027-iss7.pdf)
329 [datasheets/windsonic-1405-027-iss7.pdf](http://gillinstruments.com/data/datasheets/windsonic-1405-027-iss7.pdf).
- 330 GPSA. 2011. Section 1 General Information, in *Engineering Data Book, 13th Edition (Electronic) Volume I II*.
331 United States.
- 332 Grossman A. 2020. Dark Sky Has a New Home. Dark Sky. <https://blog.darksky.net/>.

- 333 Kairos. 2019. Kairos Aerospace Technical White Paper: Methane Detection. *Kairos Aerospace*
334 [http://kairosaerospace.com/wp-content/uploads/2019/09/Kairos-Aerospace-](http://kairosaerospace.com/wp-content/uploads/2019/09/Kairos-Aerospace-Methane-Detection.pdf)
335 [Methane-Detection.pdf](http://kairosaerospace.com/wp-content/uploads/2019/09/Kairos-Aerospace-Methane-Detection.pdf).
- 336 Kemp CE, Ravikumar AP, Brandt AR. 2016. Comparing Natural Gas Leakage Detection Technologies Us-
337 ing an Open-Source “Virtual Gas Field” Simulator. *Environmental Science & Technology* **50**(8): 4546–
338 4553. ISSN 0013-936X, 1520-5851. doi:10.1021/acs.est.5b06068. [https://pubs.acs.org/doi/10.](https://pubs.acs.org/doi/10.1021/acs.est.5b06068)
339 [1021/acs.est.5b06068](https://pubs.acs.org/doi/10.1021/acs.est.5b06068).
- 340 Lyon DR, Alvarez RA, Zavala-Araiza D, Brandt AR, Jackson RB, et al. 2016. Aerial Surveys of Elevated Hy-
341 drocarbon Emissions from Oil and Gas Production Sites. *Environmental Science & Technology* **50**(9): 4877–
342 4886. ISSN 0013-936X, 1520-5851. doi:10.1021/acs.est.6b00705. [https://pubs.acs.org/doi/10.](https://pubs.acs.org/doi/10.1021/acs.est.6b00705)
343 [1021/acs.est.6b00705](https://pubs.acs.org/doi/10.1021/acs.est.6b00705).
- 344 NOAA. 2020. High Resolution Rapid Refresh (HRRR) CONUS 2-D Fields GRIB2 Table Documentation. *National*
345 *Oceanic and Atmospheric Administration* [https://rapidrefresh.noaa.gov/hrrr/HRRRv4_](https://rapidrefresh.noaa.gov/hrrr/HRRRv4_GRIB2_WRFTWO.txt)
346 [GRIB2_WRFTWO.txt](https://rapidrefresh.noaa.gov/hrrr/HRRRv4_GRIB2_WRFTWO.txt).
- 347 Omara M, Zimmerman N, Sullivan MR, Li X, Ellis A, et al. 2018. Methane Emissions from Natural Gas Production
348 Sites in the United States: Data Synthesis and National Estimate. *Environmental Science & Technology* **52**(21):
349 12915–12925. ISSN 0013-936X, 1520-5851. doi:10.1021/acs.est.8b03535. [https://pubs.acs.org/](https://pubs.acs.org/doi/10.1021/acs.est.8b03535)
350 [doi/10.1021/acs.est.8b03535](https://pubs.acs.org/doi/10.1021/acs.est.8b03535).
- 351 PG&E. 2019. California Gas Transmission | Pipe Ranger | Operating Data | Gas Quality. *Pacific Gas and Electric*
352 *Co* https://www.pge.com/pipeline/operations/gas_quality/index.page.
- 353 Ravikumar AP, Sreedhara S, Wang J, Englander J, Roda-Stuart D, et al. 2019. Single-blind Inter-comparison of
354 Methane Detection Technologies - Results from the Stanford/EDF Mobile Monitoring Challenge. *Elementa:*
355 *Science of the Anthropocene* **7**(37): 29. doi:10.1525/elementa.373. [https://www.elementascience.](https://www.elementascience.org/articles/10.1525/elementa.373/)
356 [org/articles/10.1525/elementa.373/](https://www.elementascience.org/articles/10.1525/elementa.373/).
- 357 Ravikumar AP, Wang J, McGuire M, Bell CS, Zimmerle D, et al. 2018. “Good versus Good Enough?” Em-
358 pirical Tests of Methane Leak Detection Sensitivity of a Commercial Infrared Camera. *Environmental Sci-*
359 *ence & Technology* **52**(4): 2368–2374. ISSN 0013-936X, 1520-5851. doi:10.1021/acs.est.7b04945. [https:](https://pubs.acs.org/doi/10.1021/acs.est.7b04945)
360 [//pubs.acs.org/doi/10.1021/acs.est.7b04945](https://pubs.acs.org/doi/10.1021/acs.est.7b04945).
- 361 Schivley G, Azevedo I, Samaras C. 2018. Assessing the evolution of power sector carbon inten-
362 sity in the United States. *Environmental Research Letters* **13**(6): 064018. ISSN 1748-9326. doi:
363 10.1088/1748-9326/aabe9d. [http://stacks.iop.org/1748-9326/13/i=6/a=064018?key=](http://stacks.iop.org/1748-9326/13/i=6/a=064018?key=crossref.5142b181a7ebcbef80ae62dccf3b75fe)
364 [crossref.5142b181a7ebcbef80ae62dccf3b75fe](http://stacks.iop.org/1748-9326/13/i=6/a=064018?key=crossref.5142b181a7ebcbef80ae62dccf3b75fe).
- 365 Schwietzke S, Harrison M, Lauderdale T, Branson K, Conley S, et al. 2019. Aerially guided leak detec-
366 tion and repair: A pilot field study for evaluating the potential of methane emission detection and
367 cost-effectiveness. *Journal of the Air & Waste Management Association* **69**(1): 71–88. ISSN 1096-2247,
368 2162-2906. doi:10.1080/10962247.2018.1515123. [https://www.tandfonline.com/doi/full/](https://www.tandfonline.com/doi/full/10.1080/10962247.2018.1515123)
369 [10.1080/10962247.2018.1515123](https://www.tandfonline.com/doi/full/10.1080/10962247.2018.1515123).
- 370 Sierra. 2019. Sierra: QuadraTherm 780i. *Sierra Instruments* [https://www.sierrainstruments.com/](https://www.sierrainstruments.com/products/quadratherm/780i.html)
371 [products/quadratherm/780i.html](https://www.sierrainstruments.com/products/quadratherm/780i.html).
- 372 Zavala-Araiza D, Lyon DR, Alvarez RA, Davis KJ, Harriss R, et al. 2015. Reconciling divergent estimates of oil
373 and gas methane emissions. *Proceedings of the National Academy of Sciences* pp. 201522126. ISSN 0027-
374 8424, 1091-6490. doi:10.1073/pnas.1522126112. [http://www.pnas.org/lookup/doi/10.1073/](http://www.pnas.org/lookup/doi/10.1073/pnas.1522126112)
375 [pnas.1522126112](http://www.pnas.org/lookup/doi/10.1073/pnas.1522126112).